Journal of Materials Processing Technology, Volume 265, March 2019, pp. 201-209
DOI: 10.1016/j.jmatprotec.2018.10.023

Investigation of process factors affecting mechanical properties of INCONEL 718 superalloy in wire + arc additive manufacture process

Xiangfang Xu*, Jialuo Ding, Supriyo Ganguly, Stewart Williams

Welding Engineering and Laser Processing Centre, Cranfield University, Bedford, MK43 0AL, UK

Abstract: This paper systematically evaluated the effect of oxide, wire source and heat treatment on the mechanical properties of wire + arc additively manufactured (WAAM) INCONEL 718. Comparison of the as deposited grain structure was made with laser-powder based AM and wrought INCONEL 718. Results showed that oxides formed during deposition had no effect on the mechanical properties since a 0.5μm thick passivation layer consisting of Cr_2O_3 and Al_2O_3 formed upon deposition and prevented further oxides from forming inside the bulk. Wires from different suppliers resulted in around 50 MPa difference in UTS possibly due to the slight compositional variation and uncertainties in TiN inclusion. Standard heat treatment improved the strength from 824 MPa to 1110 MPa in the horizontal direction, but the average strength was 105 MPa lower than the wrought alloy. The as deposited WAAM INCONEL718 featured large columnar grains and numerous Laves phase, as compared to the fine grains of laser powder bed fusion and wrought INCONEL 718. This starting microstructure led to less favourable and less numerous precipitates forming during heat treatment, which is the main reason for the strength mismatch. A different heat treatment would not help due to the starting microstructure.

Keywords: INCONEL 718; wire + arc additive manufacture; mechanical properties; heat treatment; oxide

* Corresponding author.
E-mail address: xiangfang.xu@cranfield.ac.uk (X. Xu).

1. Introduction

INCONEL 718 superalloy (IN718) is an age-hardenable Ni-Cr austenitic material with a wide service temperature range from -257°C to 704°C (Special Metals, 2007). Since IN718 was developed in the 1960s, the combination of high tensile, fatigue and creep-rupture strength, excellent oxidation resistance and outstanding resistance to postweld cracking has made IN718 the most widely used Ni-based superalloy in aircraft engine history (Qi et al., 2009).

Since IN718 is an important but expensive material widely used in various sectors, cost-effective manufacturing methods are required to ease machining, reduce material wastage, enhance design freedom, and shorten lead-times. Metal additive manufacturing (AM) offers these benefits through the manufacturing principle of depositing materials in a layer-by-layer manner according to a CAD model to achieve a near net-shaped component. So far, various AM techniques have been applied to IN718, particularly in laser-powder based AM process including laser powder bed fusion (PBF) and laser direct metal deposition (DMD) process. The tensile properties of the PBF IN718 were found to be equivalent or superior to the wrought alloy after heat treatment (Zhang et al., 2015). However, the laser-powder AM parts were frequently associated with porosity (relative density 98.4% % (Jia and Gu, 2014)) and unmelted powder particles issues (Blackwell, 2005), depending highly on powder source and process parameters. Although hot isostatic pressing (HIP) proved to be able to solve these issues, it would also coarsen the grain size substantially (Zhong et al., 2016). Besides, production quantity and component dimension are the limiting factors of the PBF process (Trosch et al., 2015). Wire + Arc Additive Manufacture (WAAM) is an AM process that has high deposition rate and suitable for large-scale components as an electric arc is used as the heat source and wire as the feedstock (Cong et al., 2014; Williams et al., 2015). Initial WAAM studies using MIG (Clark et al., 2008) and TIG (Asala et al., 2017; Baufeld, 2012) proved the feasibility of depositing simple IN718 features; however, the effect of heat treatment was not investigated

and the relationship between the deposition process and the material properties is yet to be studied.

Mechanical properties are a major concern for WAAM IN718 before its implementation in industry. Therefore more fundamental research is required to gain an understanding of how the critical factors in AM processes can affect the mechanical properties of the final product. Mechanical properties of an alloy are determined by the defects (porosities and inclusions), alloying chemistry, microstructure, and heat treatment, depending on the strengthening mechanism of the particular alloy. Porosity is usually not an issue for most of the WAAM alloys, excluding aluminium alloys (Gu et al., 2016), since the feedstock is fully melted during deposition to form a fully-dense component.

(Mitchell, 1991) reported that control of the oxide, one of the major inclusion types, was crucial for producing high-quality IN718 bulk, and oxygen level should be less than 3ppm to minimise the oxide precipitation at temperatures above the liquidus. However, WAAM is an open building process, and the environment contains sufficient oxygen; even when using additional global shielding (Xu et al., 2017), the oxygen level can still be above a few hundred ppm. WAAM features a big melt pool, slow cooling rate (as compared to PBF process, and limited heat conduction route; besides, the low thermal conductivity of IN718 (11.4 W/mK (MatWeb Web Page, n.d.)) leads to more prolonged exposure time of the high-temperature deposit to the surrounding environment, all of which makes oxidation during WAAM IN718 inevitable. (Xu et al., 2018a) presented that in the WAAM maraging steel, oxide particles were found to be dispersed inside the bulk and resulted in the decrease in elongation. IN718, in particular, is known to be sensitive to an oxidation assisted crack growth mechanism (Molins et al., 1997), and the oxide film in IN718 has poor wetting with the parent metal and could contribute to a lack of bonding or a crack, as explained by (Zhang et al., 2013). So far, it is not clear if the

oxide would enter the bulk during WAAM process of IN718 and effect of the oxide on the mechanical properties of WAAM IN718 is yet to be investigated.

The feedstock can be another source of inclusions. In laser-powder based AM process, the powder source was reported to influence the product quality: (Zhao et al., 2008) deposited IN718 using gas atomized (GA) and plasma rotation electrode preparation (PREP) powders respectively and found that the former gave lower ductility due to the hollow particles resulting in porosities in the as-deposited material. In the case of WAAM, the feedstock wire currently used is an off-the-shelf product which is commercially designed for welding purposes (Williams et al., 2015). Wires provided by various suppliers may have slightly different chemical compositions and contain different level of defects. As an age hardenable alloy, the content of the hardening constituents in IN718 determines the upper limit of the quantity of the precipitates that can form in the metallurgical system, which further determines the age hardening effect and the overall mechanical properties. Hence, the effect of wires from different suppliers on the mechanical properties of the WAAM IN718 was investigated.

Heat treatment is a key requirement for IN718 in order to achieve optimum properties. IN718 gains high strength through the precipitation of various secondary phases into the austenitic matrix (γ phase) at a temperature range of 593-816°C. The most common phases include γ′ ($Ni_3(Al,Ti)$), γ" (Ni_3Nb) and metal carbides. The WAAM alloy usually has a different microstructure from the wrought alloy owing to its inherently different thermal history. Therefore it is necessary to understand how various phases precipitate and distribute during the WAAM process, and the resultant effect on the mechanical behaviour of WAAM IN718. Also, the response of WAAM microstructure to the standard heat treatment needs to be investigated.

Hence, this paper reports on the effect of key factors in the WAAM process, including oxide formation, wire variations and heat treatment, on the mechanical properties of WAAM IN718.

A comparison will be made between the IN718 produced by WAAM, laser-powder based AM and wrought process.

2. Experimental

2.1 Setup and deposition procedures

Fig. 1 shows the WAAM setup for IN718 deposition. Cold metal transfer (CMT), a variant of metal inert gas (MIG) welding process featuring high deposition rate and low heat input (Xu et al., 2018b), is selected as the heat source. The WAAM system consisted mainly of a CMT power source (Fronius, VR 7000), a CMT torch, a wire feeder and a 6-axis ABB robot for controlling the deposition path.

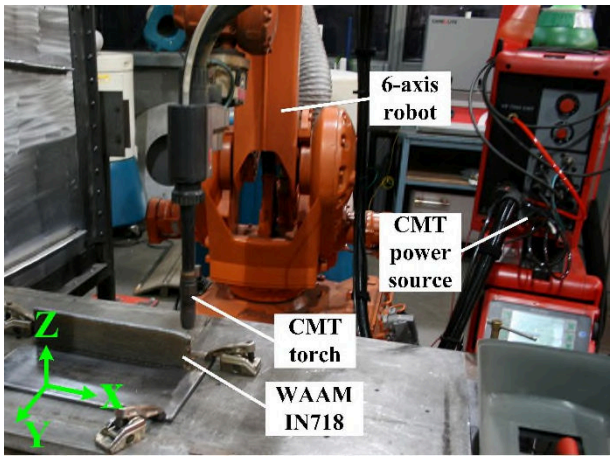

Fig. 1. Experimental setup of WAAM system (X-along wall length, Z-along wall height).

For the oxide study, two comparative linear wall structures (54 layers) were deposited: one built in a normal layer-by-layer manner regardless of the oxide formation; the other was applied mechanical grinding using an angle grinder to completely remove the oxides formed on the top deposit before the next deposition (removal thickness around a few microns). The wire used for this study is labelled Wire A (1.2mm, conforming to AMS5832E). Deposition parameters are as follows: contact tip-to-work distance (CTWD)=14mm, wire feed speed (WFS)=7m/min,

deposition torch travel speed (TS)=6mm/s, layer height=2.8mm, shielding gas flow rate=15l/min, and interpass cooling time=3mins.

For wire source study, Wire B (1.2mm, conforming to AMS 5832) from a different supplier was used to deposit the third wall with identical process parameters. No interpass grinding was applied. The elemental composition of the wires was measured using energy dispersive spectrometry (EDS); to minimise the measurement error, the entire transverse cross-section of the wire was divided into ten segments, and a full EDS analysis was carried out for each segment to compute the average elemental composition, as shown in Table 1.

Table 1. Elemental composition of the wires (wt. %).

	Ni	Cr	Nb+Ta	Mo	Ti	Al	Co	Mn	Fe
Wire A	52.3	18.81	5.33	3.2	0.96	0.53	0.35	0.15	Bal.
Wire B	53.15	19.42	5.22	2.95	0.96	0.47	0.41	0.11	Bal.

2.2 Heat treatment

The industrial standard heat treatment conforming to Aerospace Material Specifications (AMS) was applied to WAAM IN718, as described in Table 2. Before solution treatment, all samples underwent a 10mins ultrasonic bath in acetone for degreasing; then samples were thoroughly rinsed using clean water and dried before putting into the furnace. A piece of wrought IN718 alloy conforming to AMS 5596 specification was applied the identical heat treatment for comparison. The thermal history of the samples during heat treatment was monitored by attaching a thermal couple to a sample, and an oscilloscope (Yokogawa DL750 ScopeCorder) was used to record the temperature data (sample rate 5S/s).

Table 2. Heat treating procedure applied in this study (AMS-5662M for forged IN718).

Step 1-Solution	hold at 970-980°C for 1h
Step 2-Aging	hold at 718°C for 8h; furnace cool to 620°C, hold for 8h

2.3 Analytical methods

Samples were cross-sectioned, mounted, ground, and polished before further analysis. The microstructure was revealed by electrolytic etching in 10% oxalic acid solution using 6V for 10s. Morphology of the oxides, grain boundaries and secondary phases was observed using an optical microscope (OM) and scanning electron microscopy (SEM, FEI XL30-SFEG). EDS (Oxford Instrument) was used for elemental analysis, and electron back-scatter diffraction (EBSD) analysis was applied to characterise the grain structure. Microhardness test was performed using Zwick/Roell hardness tester under a load of 1 kg and holding time of 15s.

Tensile test coupons were extracted along both horizontal (X) and vertical direction (Z) using the material leaving out 20mm from both ends and 10mm from the top and the substrate. Machining was carried out after heat treatment. The coupons are milled to a dog-bone shape according to BS EN 2002-1:2005 standard in a non-proportional manner with a gauge length of 24mm, as shown in Fig. 2. The room temperature tensile test was conducted on an Instron 5500R electromechanical testing machine with a load cell of 100kN and a crosshead speed of 1mm/min. For each condition, at least three samples were tested.

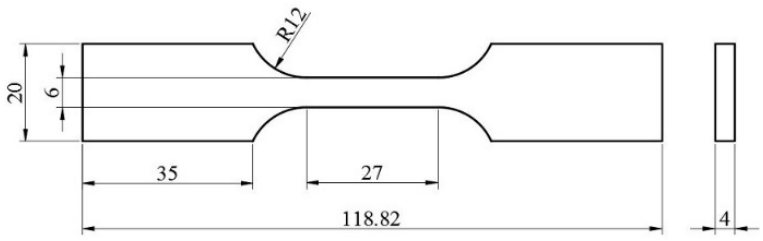

Fig. 2. Tensile coupon dimensions.

3. Results

3.1 Effect of oxide

3.1.1 Oxide formation and accumulation

Fig. 3a shows the comparison of the top deposit before and after mechanical grinding; after grinding the oxide layer is entirely removed and the shining fresh alloy is exposed for the next deposition. Fig. 3b shows numerous discrete oxide islands formed immediately after one more deposition on the oxide-free surface. As can be seen, the oxide formation is so active that one deposition is enough to produce the oxides that almost entirely covers the top deposit. The left side in Fig. 3a shows the final oxide layer formed on the top deposit in the normally built wall (without intermediate grinding): the discrete oxide islands observed in Fig. 3b are replaced by an entire thin oxide layer which is very smooth and coherent to the pure alloy.

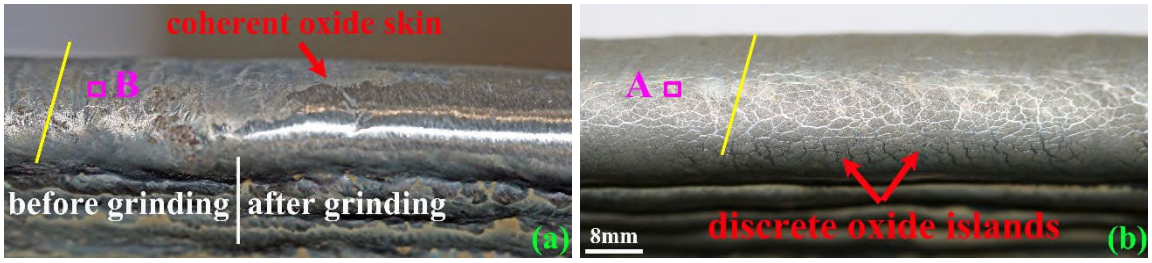

Fig. 3. (a) Final oxide layer formed on the topmost deposit in the normally built WAAM IN718 wall (b) oxide islands formed after one deposition on the oxide-free surface.

Fig. 4 shows the SEM images of Zone A and B in Fig. 3, representing the morphology of the oxide layer when it forms after one deposition and after 54 times deposition respectively. In the oxide layer formed after one layer deposition (Fig. 4a), numerous individual oxide particles of complex compositions (Area C in Table 3) are observed and do not fully cover the surface of the pure metal (Area D in Fig. 4a). By contrast, after 54 layers deposition, the oxide islands join together to form a dense and smooth skin showing a networked morphology (Zone E in Table 3), which fully covers the pure alloy.

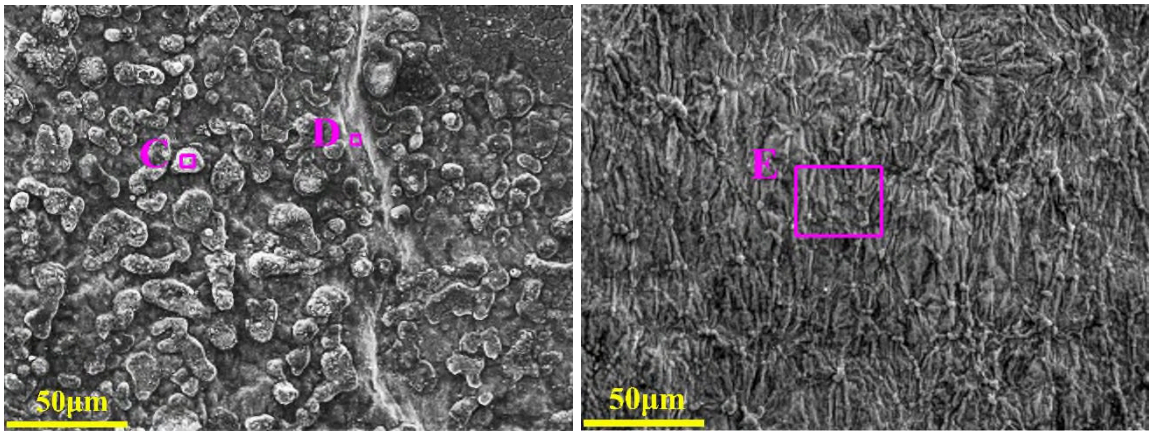

(a) Zone A (b) Zone B

Fig. 4. SEM images of Zone A and B in Fig. 3 showing the oxide morphology.

Fig. 5 compares the thickness of the oxide layer near the top of the wall shown in Fig. 3. In the oxide layer formed after one deposition (Fig. 5b), discrete oxide islands are observed with a random thickness, and some could reach up to 2μm. After 54 layers of deposition, the uniform oxide layer possesses a thickness of around 0.5μm, indicating that there is no oxide accumulation happening during the layer-by-layer deposition process.

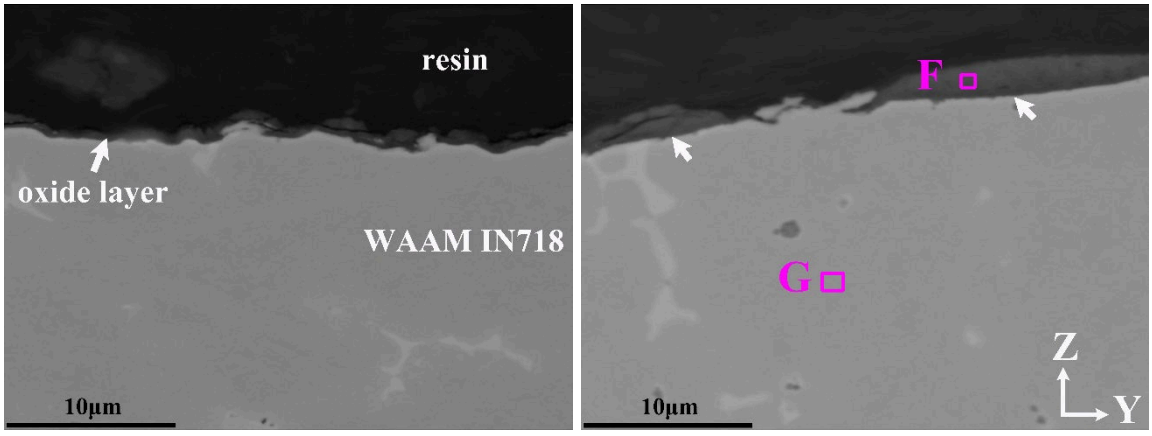

(a) wall in Fig. 3a (b) wall in Fig. 3b

Fig. 5. SEM images of the oxide layer at the top of the walls shown in Fig. 3 (yellow line in Fig. 3 indicates the sectioning position).

Table 3. EDS results of the selected areas (wt. %).

	O	Al	Si	Ti	Cr	Fe	Ni	Nb	Mo
C	35.79	17.69	0.24	15.83	8.75	5.66	13.9	2.13	-
D	15.06	12.55	-	3.84	13.71	13.25	35.83	3.73	2.02
E	28.37	21.39	-	4.11	8.39	7.4	21.68	8.65	-
F	39.6	41.44	0.49	5.83	3.07	1.89	5.02	3.19	-
G	-	0.63	0.18	0.89	19.64	18.66	53.15	4.08	2.77

Fig. 6 shows the microhardness variation of the two comparative walls measured from the top towards the substrate. Despite the small fluctuation, the microhardness of the two walls is generally identical along the height direction with a negligible average value difference of 1HV, which indicates that oxides are very unlikely to be embedded in the matrix and harden the matrix.

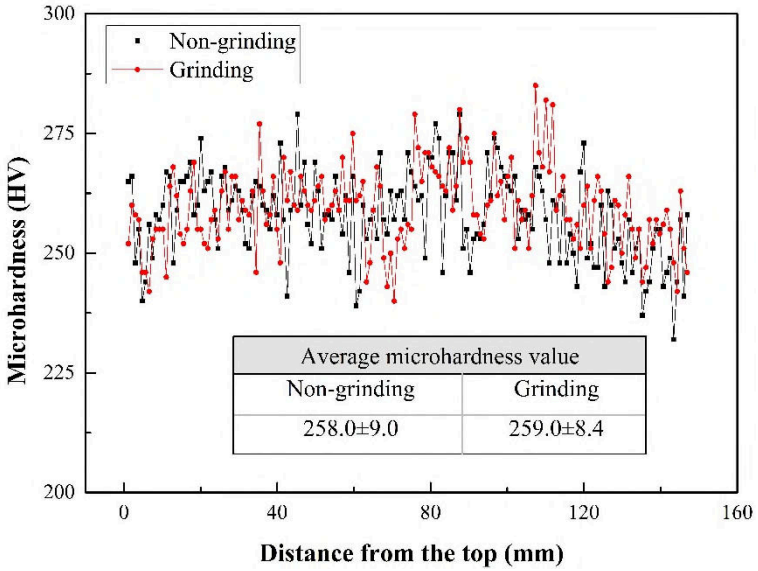

Fig. 6. Microhardness of the two comparative walls built with and without grinding.

3.1.2 Mechanical properties

Fig. 7 shows the as deposited WAAM IN718 wall structure and the location where the tensile samples were extracted. The sample position numbering was applied to both walls. A detailed

comparison of the tensile test results is presented in Fig. 8 and Table 4. From Fig. 8, it is found that at each corresponding position, the ultimate tensile strength (UTS), 0.2% yield strength (0.2%YS) and elongation value for the two walls are almost the same. From Table 4, after grinding each layer, the change in the average UTS, 0.2%YS and elongation is also negligible.

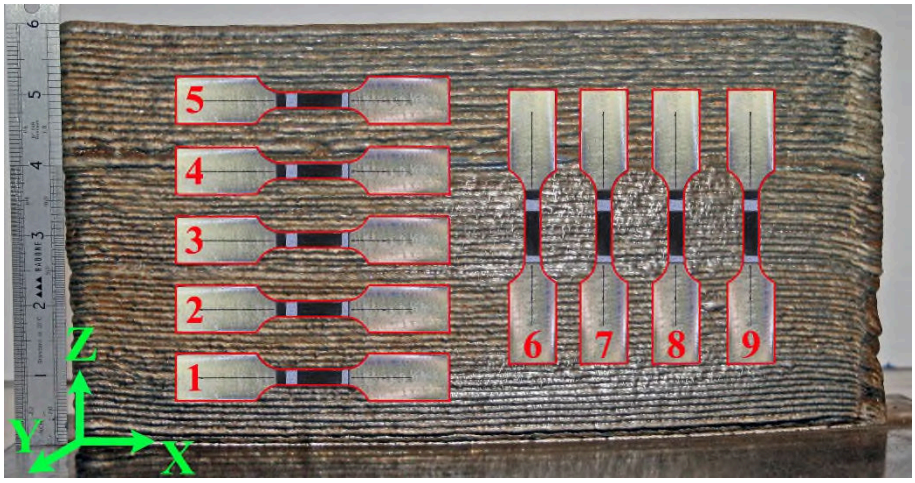

Fig. 7. WAAM IN718 wall structure and the sample extraction positions.

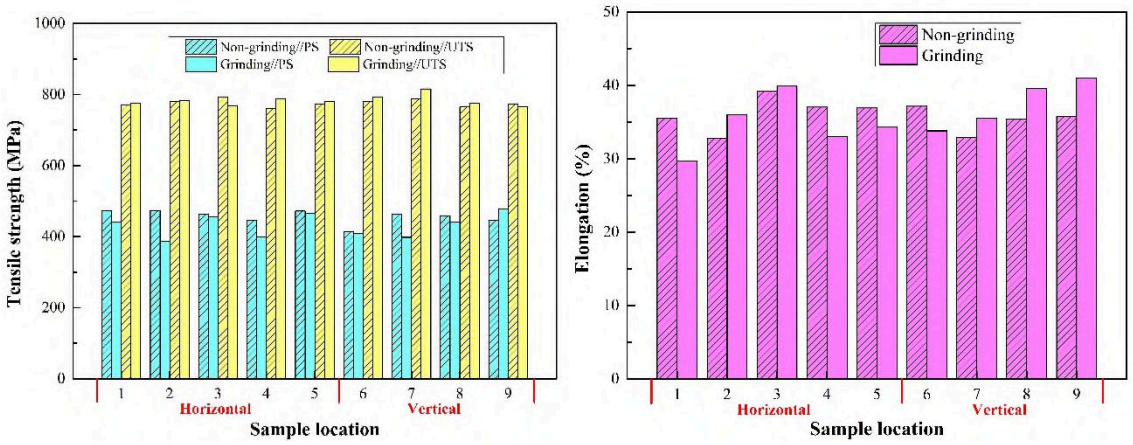

(a) UTS and 0.2%YS (b) elongation

Fig. 8. Mechanical testing results of the walls deposited with and without interpass grinding.

Table 4. Tensile test results of the WAAM IN718 on average.

			UTS / MPa		0.2%YS / MPa		Elongation / %	
			H	V	H	V	H	V
WAAM-AD	Wire A	Non-grinding	776±10	777±8	466±10	446±19	36.3±2.1	35.3±1.6
		Grinding	779±7	787±19	429±31	431±31	34.6±3.4	37.5±2.9
	Wire B	Non-grinding	824±15	832	514±17	416	34.0±0	30.9
WAAM-SA	Wire B	Non-grinding	1110±3	1233±16	807±1	889±5	15.5±0.3	19.4±2.8

AD-as deposited; SA-solution plus aging; H-horizontal; V-vertical.

3.2 Effect of wire

Table 4 also presents the tensile properties of WAAM IN718 deposited using two different wires. As can be seen, the average UTS obtained using Wire B is 48MPa and 55MPa higher than using Wire A in the horizontal and vertical direction respectively, but the elongation achieved is 2.3% and 4.4% lower respectively. Both UTS values are inferior to the casting standard (862MPa, see Table 5), but the ductility is considerably superior to the castings.

3.3 Effect of heat treatment

Fig. 9 shows the thermal history recorded during heat treatment. The real temperature for solution and double aging is 966.1°C, 713.3°C and 616.6°C respectively, which generally complies with the standard shown in Table 2.

From Table 4, the heat treatment results in a 286MPa (increased by 34.7%) and 401MPa (increased by 48.2%) increase in UTS along the horizontal and vertical direction respectively; while the elongation is observed an 18.5% and 11.5% decrease respectively. The highest individual UTS obtained is in the vertical direction, being 1248MPa which is very close to the wrought alloy (1276 MPa); however, the average strength of the heat treated WAAM IN718 is 105MPa lower than the wrought alloy.

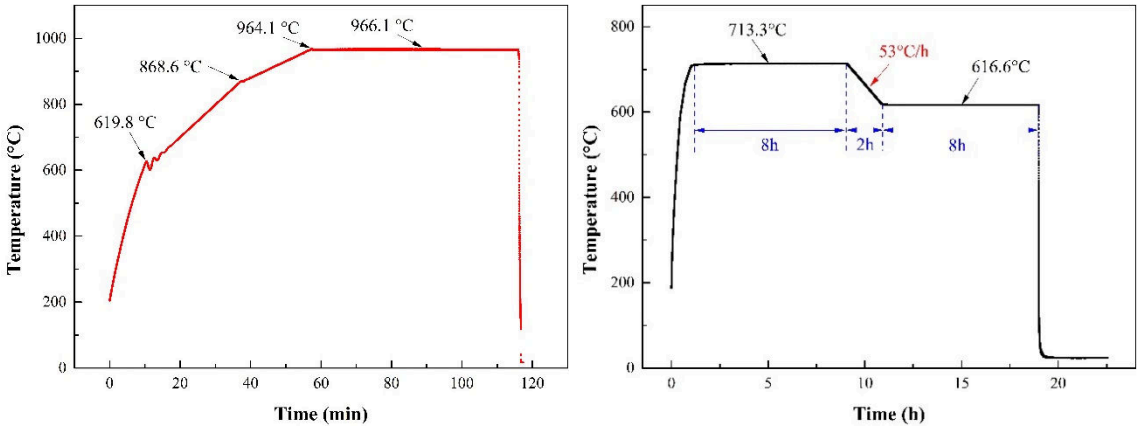

(a) solution (b) aging

Fig. 9. Real thermal history during heat treatment.

4. Discussion

4.1 Oxide characteristics

From Fig. 5b and Table 3 (Area F), the oxides formed in the WAAM IN718 are mostly a mixture of Al (41.44 wt.%) and Cr (3.07 wt.%) oxides (Al_2O_3 and Cr_2O_3 according to (Wang and Chen, 2006)), and Mo is absent in the oxide. IN718 essentially gains oxidation resistance through a passivation process, i.e., the formation of a protective Chromia (Cr_2O_3) scale. Though at the temperature higher than 1000°C the formation of volatile Cr_2O_3 results in a loss of the protective scale (Greene and Finfrock, 2001), the Al_2O_3 provides adequate oxidation resistance since Al_2O_3 resists spalling at temperatures up to 1300-1350°C (Wang and Chen, 2006). Since the oxides are of a lower density than the pure metal, it flows onto the top of the melt pool upon formation and solidifies as a protective shell to prevent the successive oxides from the formation. When there is only one deposition, the oxide forms as discrete islands and the quantity is not enough to fully cover the top deposit; the gaps between these islands expose the pure alloy to oxygen upon successive depositions to allow more oxides to form until they join together and firstly fully cover the top deposit to prevent further oxide formation. Due to the lack of ongoing oxide formation, no oxide accumulation is observed during the WAAM of

IN718. Besides, the characteristic of oxides in IN718 being dense prohibits oxygen diffusion through the oxide layer to the parent metal; thereby oxides are not found inside the bulk.

4.2 Uncertainties from the wire

From Table 1, the elemental composition varies slightly between suppliers, with Wire B having a slightly lower content of Nb and Al. The content of alloying elements, especially the hardening constituents, is critical for age-hardenable alloys when strength is of interest. For some alloying systems, even slight difference in element composition could make a difference to the strengthening effect. In IN718, for example, (Radhakrishna and Prasad Rao, 1997) reported that reducing Nb content in the wire helped control the Laves phase formation and ease the homogenization process.

There could also be uncertainties in non-metallic inclusions in the wire. The thermochemistry of IN718 results in two types of inclusions, TiN and Al_2O_3, which not only influence the mechanical properties but also the solidification structure (Mitchell, 1989); the prior-existing TiN particles act as the principal nucleation sites for NbC (which is usually an undesired carbide according to (ASM International, 1990)) during solidification since they are isomorphous (Mitchell, 2010). Fig. 10 shows a TiN inclusion (the dark phase) observed in Wire B. The same type of inclusion is also observed in Wire A. Fig.11 presents the inclusion found in the fracture surface of the WAAM IN718 built using Wire B, which is identified as TiN through EDS analysis and proves that the inclusions also go into the WAAM alloy.

The different mechanical properties using different wires are most likely due to the compositional difference (possibly Nb) since a strength increase and ductility decrease are both observed when using Wire B; defects, such as inclusions, usually results in a reduction in both properties. However, the extreme complexity in the IN718 metallurgy makes it difficult to directly correlate the slight variations in wire composition and TiN inclusion content with the

mechanical behaviour; also, accurately quantifying the variations between the wires is difficult given that there could be significant variations along the length of the wire. The present results indicate that the wire source could be a key factor that affects the mechanical properties of the WAAM alloy, which is possibly because wires from different manufacturers do not have an identical chemical composition and inclusion level.

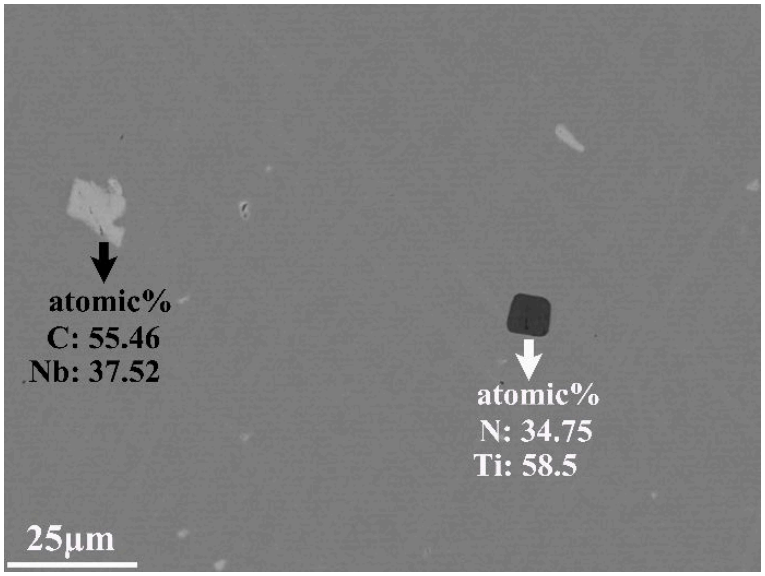

Fig. 10. Inclusions observed in Wire B.

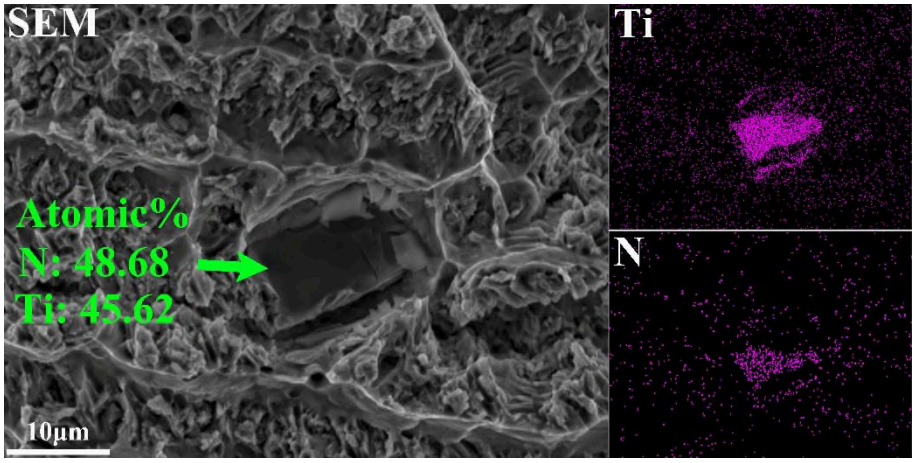

Fig. 11. TiN inclusion found in the fracture surface of the WAAM IN718 built using Wire B.

4.3 Mechanical properties

4.3.1 Comparison with other AM products

Table 5 summarises the mechanical properties of IN718 obtained using various AM processes. The WAAM IN718 possesses essentially the same strength as shaped metal deposition (SMD, using gas tungsten arc process) product, but the elongation is much higher (32.9% against 28%), which is possibly due to the different heat input, wire variations and tensile coupon design (bar with the dimension of 25×8×3mm, gauge length 25mm (Baufeld, 2012)). In the as deposited condition, the strength of WAAM IN718 is slightly lower than the casting (827MPa against 862MPa), but the ductility is considerably higher (32.9% against 5%). The strength of laser-powder AM IN718 varies among literature but is generally higher than the WAAM alloy in the as deposited condition: the DMD process produces slightly higher strength (847MPa, (Zhong et al., 2016) and 904MPa, (Qi et al., 2009) against 827MPa), and the PBF process gives significantly better strength (1126MPa (Zhang et al., 2015) against 827MPa). Among all the literature WAAM generally produces the highest ductility, which is due to the slower cooling rate as compared to laser-powder based process (Baufeld, 2012).

After solution plus aging, the UTS of WAAM IN718 is 105MPa lower than the wrought alloy. However, when the same heat treatment was applied to laser-powder AM IN718, the resultant strength is superior to WAAM alloy, being 1221MPa (Qi et al., 2009), 1371MPa (Zhang et al., 2015) and 1430MPa (Trosch et al., 2015) against 1171MPa. Note that the wrought standard is 1276MPa, so the heat treatment generally works well for PBF IN718, but less effective for DMD product (Qi et al., 2009).

Table 5. Comparison of the strength of IN718 produced by various AM process (on average).

	UTS / MPa	0.2%YS / MPa	Elongation / %
WAAM★-AD	827±13	482±48	32.9±1.5
WAAM★-SA	1171±62	848±41	17.4±2.8
SMD-AD (Baufeld, 2012)	828±8	473±6	28±2
DMD-AD (Zhong et al., 2016)	847	525	29
DMD-AD (Qi et al., 2009)	904	552	16.2
DMD-SA (Qi et al., 2009)	1221	1007	16
PBF-AD (Zhang et al., 2015)	1126	849	22.8
PBF-SA (Zhang et al., 2015)	1371	1084	10.1
PBF-SA (Trosch et al., 2015)	1430	1185	18.6
Casting AMS5383	862	758	5
Wrought AMS5662	1276	1034	12

★ *using Wire B*

4.3.2 Explanation of the inferior mechanical properties

4.3.2.1 Grain morphology

Since the precipitation behaviour during heat treatment is determined by the starting grain structure, it is relevant to compare the grain structure of the as deposited WAAM IN718 with the wrought alloy, as shown in Fig. 12. The WAAM alloy shows columnar grain boundaries typical of the WAAM process, as indicated by the green arrows in Fig. 12a (grain boundary depicted for better visibility); the thickness of the columnar grain can be as big as 200 μm at the half height position of the wall structure. The same large columnar grain structure is also observed in the WAAM Ti6Al4V as a result of the epitaxial growth due to the directional heat flow (Martina et al., 2015). In contrast, the wrought alloy shows a finely equiaxed grain structure with the average grain size of 7.5 (ASTM E112, 26.7 μm). Fig. 13 presents the EBSD grain map of the as deposited WAAM IN718 wall structure right above the substrate; numerous columnar grains show a directional growth along the building direction (Z) which is also the

heat flow direction. Thanks to the higher cooling rate due to the presence of the substrate, the columnar grains are smaller as compared to those observed at the half height (Fig. 12a), with the thickness varying between 50-150μm and the length being comparable to the whole map.

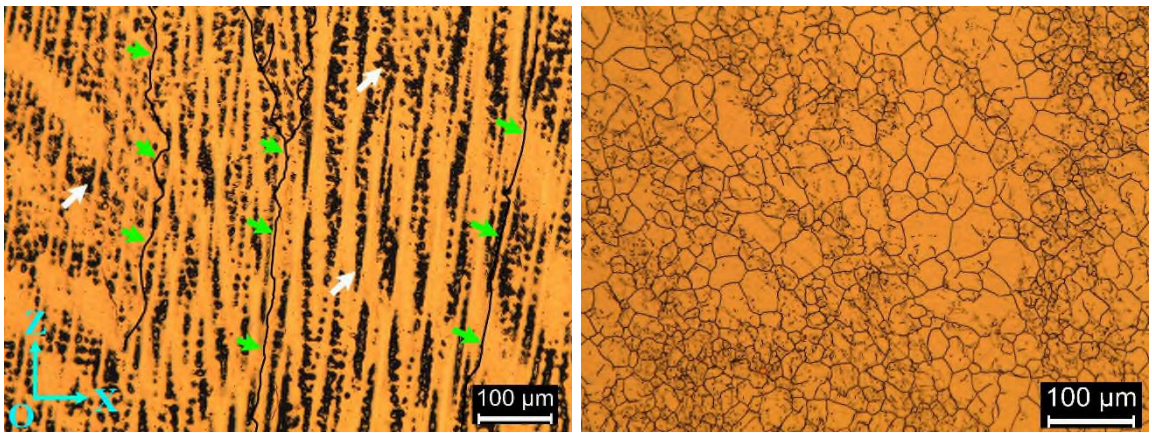

(a) WAAM (as deposited, half height of the wall) (b) wrought (solutionized)

Fig. 12. Grain boundaries of IN718 produced by WAAM and wrought process.

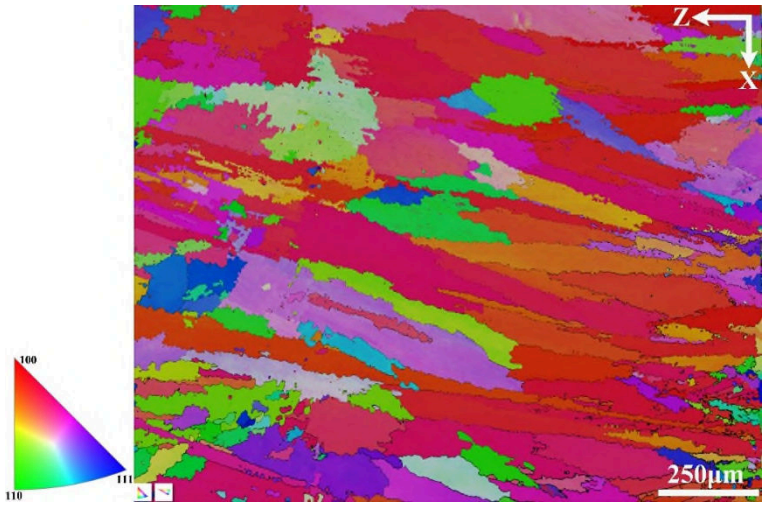

Fig. 13. EBSD orientation map showing the columnar grains near the bottom of the WAAM IN718 wall structure in the as deposited condition.

After solution treatment, the WAAM grain structure ready for subsequent aging is much coarser as compared to the as deposited alloy in Fig. 12a. So the grains have greater thickness and less grain boundary area compared to the wrought alloy. The superiority of the PBF IN718

in the heat treated condition compared to the wrought material was due to the fine grains and small dendrite arm spacing resulting from the high cooling rate (Qi et al., 2009); according to (Trosch et al., 2015), the grain size (around 4μm) was 10 times and 100 times finer than the forged (around 50μm) and cast (around 800μm) microstructure respectively. Note that precipitation of the secondary phases at the grain boundaries is more effective in strengthening; the lack of grain boundaries in the WAAM IN718 due to the large columnar grains makes such precipitation less likely to happen, as compared with the finely equiaxed grains in the wrought alloy.

4.3.2.2 Precipitates

(Brand et al., 1996) reported that the chemical composition, distribution, location and possible coagulation during the thermal and mechanical treatments are decisive in the microstructural and mechanical properties development in IN718.

Fig. 14 presents the SEM micrographs of the precipitates formed in response to the heat treatment. In the wrought IN718 (Fig. 14b), the nanosized precipitates are found to embed and disperse uniformly throughout the matrix. Particularly at the grain boundaries, the hardening phases are observed to precipitate in either spherical shape or needle shape (indicated by pink arrows in Fig. 14b) with the length filling and orienting along the grain boundary, which serves as the impediment of grain boundary migration to strengthen the material.

In contrast, the precipitates in the WAAM 718 are found to be of different morphology and distribute much less uniformly. After heat treatment, most of the Laves phase has been transformed to the acicular δ phase which tends to cluster where the previous Laves phase is located and shows an overall directional distribution. Numerous secondary phase islands (indicated by yellow arrows in Fig. 14a) as big as 10μm are observed which are complex

mixtures of the newly formed precipitates and the untransformed Laves phase (Qi et al., 2009). Besides, no obvious grain boundaries are observed even at a lower magnification (Fig. 14a).

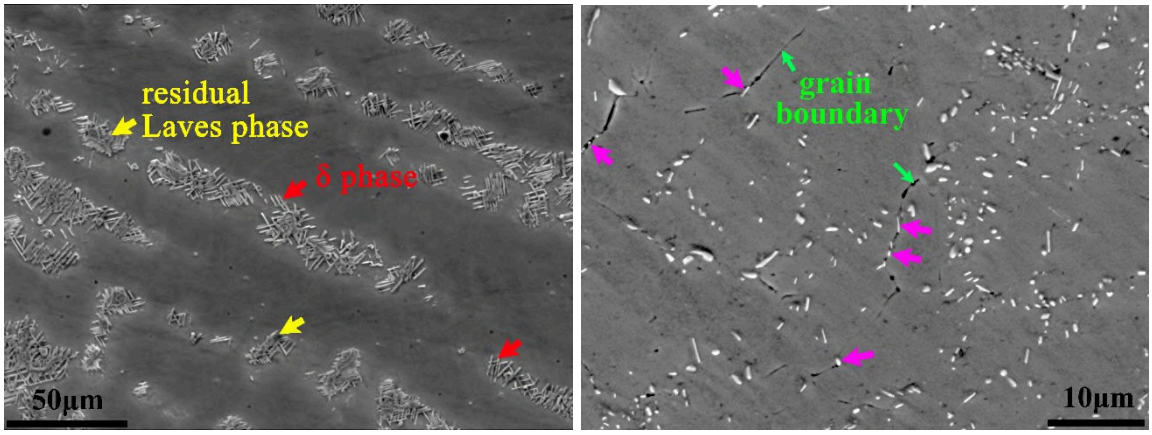

(a) WAAM (b) wrought

Fig. 14. SEM images showing the precipitates morphology and distribution in the WAAM IN718 and wrought IN718 after aging.

4.3.2.3 Heat treating standard

IN718 derives excellent mechanical properties from precipitation hardening, and the hardening effect of the precipitates depends on their type, quantity, morphology, size, and location, which is a result of the heat treatment (time, temperature and cooling method) and the starting grain structure. For proper aging to take place, the aging constituents (Al, Ti, and Nb) must be in solution first; if they are precipitated as some other phase, the full strength will not be attained. According to (Special Metals, 2007), the heat treating procedure applied in the present study produces the highest room-temperature tensile strength of wrought IN718. Many variants of this procedure have been developed to suit different starting grain structure. For example, homogenisation (see Table 6) is applied before SA in cast IN718 to minimise the elemental segregation and dissolve undesired phases, and HIPing is adopted before SA in DMD process to eliminate the unmelted powder particles and porosity (Blackwell, 2005). Even though

various heat treatment gives different mechanical behaviour, simply applying a different heat treatment would not make a difference in this study for the following two reasons.

Firstly, the starting grain structure cannot be improved simply by heating when mechanical working is absent. A finely equiaxed grain structure is desired for good mechanical behaviour; however, the WAAM alloy features larger columnar grains which, when heated to high temperature and held for some period will only to coarsen. The resultant grain structure is still not favourable for subsequent heat treatment.

Secondly, eliminating the Laves phase and avoiding grain coarsening is contradictory. On the one hand, Nb and Mo segregation are inevitable during the solidification process due to the inherent thermal conduction and non-equilibrium thermal cycles experienced in the WAAM process, which leads to the formation of detrimental Laves phases at the interdendritic area (Xiao et al., 2017). On the other hand, the normal solution temperature is not high enough to promote sufficient Nb diffusion and dissolve the Laves phase, as has been shown in Fig. 14a; the aging temperatures are only designed to precipitate γ′ and γ" strengthening phases in the γ matrix. In laser-powder based AM research, both homogenisation and HIPing using a higher temperature than solution treatment for a long duration (few hours) are reported to dissolve the Laves phase completely but results in considerable grain coarsening. From Table 6, HIPing restores the ductility but also results in a strength loss due to the grain growth (Blackwell, 2005), which is the same case for (Qi et al., 2009) when homogenisation is applied. Hence, it is impossible to dissolve the undesired Laves phase without causing grain coarsening.

Segregation is less severe in laser-powder based AM process due to the fast cooling rate (Blackwell, 2005). By contrast, Nb segregation would be more severe in the WAAM process due to the much lower cooling rate (Ram et al., 2005). Besides, the grain size of the PBF IN718 is much smaller than the WAAM alloy; note that the DMD process has a higher heat input and

lower cooling rate than the PBF, so the grains produced are also larger and the heat treatment works less effectively than the latter. These two factors make the starting grain structure different; thereby the same heat treatment procedure works better for the PBF IN718.

Table 6. Summary of mechanical properties of laser AM IN718 after various heat treatment.

	UTS / MPa	0.2%YS / MPa	Elongation / %
DMD-HSA (Qi et al., 2009)	1194	949	19.9
DMD-SA (Blackwell, 2005)	1436	1257	13 (reduction in area)
DMD-HIP+SA (Blackwell, 2005)	1380	1155	20.4 (reduction in area)

A-aging (without prior solution); HSA-homogenization+solution+aging (AMS-5383D for cast IN718); Homogenization-hold at 1093°C for 1-2hrs; HIP[1]-100MPa, 1160°C for 3hrs.

4.3.2.4 Future work

The current study indicates that it is difficult to make the WAAM alloy microstructurally and metallurgically identical to a wrought alloy through solidification conditions and composition alone. The large columnar grains in the WAAM IN718 lead to less favourable and numerous precipitates forming, which is the main reason for the strength mismatch. In future studies, process improvement based on thermomechanical processing may be considered to reduce the elemental segregation by promoting Nb diffusion and induce recrystallisation to produce a larger area of high-angle grain boundaries, thereby improving the mechanical behaviour.

5. Conclusions

High-quality deposits free from process defects were obtained by WAAM deposition of IN718. It was found that,

1. Coherent oxide layer consisting of Cr_2O_3 and Al_2O_3 form so actively that with one deposition they almost fully cover the deposit; oxides don't accumulate during the layer by layer building process, ending up with only 0.5μm thick after 54 layers deposition.

2. The oxide shows no effect on the mechanical properties since the protective oxide layer prevents further oxygen from entering the bulk and forming oxides in the bulk.
3. Wires from two suppliers produce a UTS difference of around 50MPa, which is most likely due to the slight difference in elemental composition.
4. The as deposited WAAM IN718 has large columnar grains with the thickness of 50-150μm near the substrate, orienting along the building direction, as opposed to the finely equiaxed grains in the wrought alloy with an average grain size of 26.7 μm.
5. The strength of the heat treated WAAM IN718 is 105MPa lower than the wrought alloy. This is mainly because the large columnar grains is not a favourable starting microstructure for heat treatment such that precipitates formed are of different types, fewer in number and less uniformly distributed compared to those found in the wrought alloy.
6. It is likely that applying a different heat treatment by varying the time and temperature will not enhance the mechanical behaviour unless thermo-mechanical working is introduced to produce a more favourable starting microstructure.

Acknowledgements

The authors wish to acknowledge the financial support from China Scholarship Council (NO. 201506680057) and the WAAMMat programme industrial partners. The authors would also like to thank Dr. Xianwei Liu, Steve Pope, Dr. Christine Kimpton and Dr. Tracey Roberts for the assistance during the metallographic and SEM analysis. The technical discussion with Dr Paul Colegrove and the support from Flemming Nielsen and Nisar Shah during the experiment is much appreciated.

References

Asala, G., Khan, A.K., Andersson, J., Ojo, O.A., 2017. Microstructural Analyses of ATI 718Plus® Produced by Wire-ARC Additive Manufacturing Process. Metall. Mater. Trans. A Phys. Metall. Mater. Sci. 48, 4211–4228. doi:10.1007/s11661-017-4162-2

ASM International, 1990. ASM Handbook: Volume 2 Properties and selection: Nonferrous alloys and special-purpose materials, ASM Handbook.

Baufeld, B., 2012. Mechanical properties of INCONEL 718 parts manufactured by shaped metal deposition (SMD). J. Mater. Eng. Perform. 21, 1416–1421. doi:10.1007/s11665-011-0009-y

Blackwell, P.L., 2005. The mechanical and microstructural characteristics of laser-deposited IN718. J. Mater. Process. Technol. 170, 240–246. doi:10.1016/j.jmatprotec.2005.05.005

Brand, A.J., Karhausen, K., Kopp, R., 1996. Microstructural simulation of nickel base alloy Incone* 718 in production of turbine discs. Mater. Sci. Technol. 12, 963–969. doi:https://doi.org/10.1179/mst.1996.12.11.963

Clark, D., Bache, M.R., Whittaker, M.T., 2008. Shaped metal deposition of a nickel alloy for aero engine applications. J. Mater. Process. Technol. 203, 439–448. doi:10.1016/j.jmatprotec.2007.10.051

Cong, B., Ding, J., Williams, S., 2014. Effect of arc mode in cold metal transfer process on porosity of additively manufactured Al-6.3%Cu alloy. Int. J. Adv. Manuf. Technol. 76, 1593–1606. doi:10.1007/s00170-014-6346-x

Greene, G. a., Finfrock, C.C., 2001. Oxidation of Inconel 718 in Air at High Temperatures. Oxid. Met. 55, 505–521. doi:10.1023/A:1010359815550

Gu, J., Ding, J., Williams, S.W., Gu, H., Ma, P., Zhai, Y., 2016. The effect of inter-layer cold working and post-deposition heat treatment on porosity in additively manufactured aluminum alloys. J. Mater. Process. Technol. 230, 26–34. doi:10.1016/j.jmatprotec.2015.11.006

Jia, Q., Gu, D., 2014. Selective laser melting additive manufacturing of Inconel 718 superalloy parts: Densification, microstructure and properties. J. Alloys Compd. 585, 713–721. doi:10.1016/j.jallcom.2013.09.171

Martina, F., Colegrove, P.A., Williams, S.W., Meyer, J., 2015. Microstructure of Interpass Rolled Wire + Arc Additive Manufacturing Ti-6Al-4V Components. Metall. Mater. Trans. A Phys. Metall. Mater. Sci. 46, 6103–6118. doi:10.1007/s11661-015-3172-1

MatWeb Web Page, n.d. IN718 from Matweb [WWW Document]. URL http://www.matweb.com/search/DataSheet.aspx?MatGUID=94950a2d209040a09b89952d45086134&ckck=1

Mitchell, a., 1991. Melting Processes and Solidification in Alloys 718-625. Superalloys 718, 625 Var. Deriv. 15–27. doi:10.7449/1991/Superalloys_1991_15_27

Mitchell, a., 1989. The Present Status of Melting Technology for Alloy 718. Superalloys 718 Metall. Appl. 1–15. doi:10.7449/1989/Superalloys_1989_1_15

Mitchell, A., 2010. Primary carbides in Alloy 718. 7th Int. Symp. Superalloy 718 Deriv. 161–167. doi:10.1002/9781118495223.ch11

Molins, R., Hochstetter, G., Chassaigne, J.C., Andrieu, E., 1997. Oxidation effects on the fatigue crack growth behaviour of alloy 718 at high temperature. Acta Mater. 45, 663–674. doi:10.1016/S1359-6454(96)00192-9

Qi, H., Azer, M., Ritter, a., 2009. Studies of Standard Heat Treatment Effects on

Microstructure and Mechanical Properties of Laser Net Shape Manufactured INCONEL 718. Metall. Mater. Trans. A 40, 2410–2422. doi:10.1007/s11661-009-9949-3

Radhakrishna, C.H., Prasad Rao, K., 1997. The formation and control of Laves phase in superalloy 718 welds. J. Mater. Sci. 32, 1977–1984. doi:10.1023/A:1018541915113

Ram, G.D.J., Reddy, A.V., Rao, K.P., Reddy, G.M., 2005. Microstructure and mechanical properties of Inconel 718 electron beam welds. Mater. Sci. Technol. 21, 1132–1138. doi:10.1179/174328405X62260

Special Metals, 2007. INCONEL alloy 718. pp. 1–28. doi:SMC-066

Trosch, T., Strößner, J., Völkl, R., Glatzel, U., 2015. Microstructure and mechanical properties of selective laser melted Inconel 718 compared to forging and casting. Mater. Lett. 164, 428–431. doi:10.1016/j.matlet.2015.10.136

Wang, C.J., Chen, S.M., 2006. Microstructure and cyclic oxidation behavior of hot dip aluminized coating on Ni-base superalloy Inconel 718. Surf. Coatings Technol. 201, 3862–3866. doi:10.1016/j.surfcoat.2006.07.242

Williams, S.W., Martina, F., Addison, A.C., Ding, J., Pardal, G., Colegrove, P., 2015. Wire+Arc Additive Manufacturing. Mater. Sci. Technol. 00, 1–7. doi:10.1179/1743284715Y.0000000073

Xiao, H., Li, S., Han, X., Mazumder, J., Song, L., 2017. Laves phase control of Inconel 718 alloy using quasi-continuous-wave laser additive manufacturing. Mater. Des. 122, 330–339. doi:10.1016/j.matdes.2017.03.004

Xu, X., Ding, J., Ganguly, S., Diao, C., Williams, S., 2018a. Oxide accumulation effects on wire+arc layer-by-layer additive manufacture process. J. Mater. Process. Tech. 252, 739–750. doi:10.1016/j.jmatprotec.2017.10.030

Xu, X., Ding, J., Ganguly, S., Diao, C., Williams, S., 2018b. Preliminary Investigation of Building Strategies of Maraging Steel Bulk Material Using Wire + Arc Additive Manufacture. J. Mater. Eng. Perform. 1–7. doi:10.1007/s11665-018-3521-5

Xu, X., Ganguly, S., Ding, J., Guo, S., Williams, S., Martina, F., 2017. Microstructural evolution and mechanical properties of maraging steel produced by wire+arc additive manufacture process. Mater. Charact. doi:10.1016/j.matchar.2017.12.002

Zhang, D., Niu, W., Cao, X., Liu, Z., 2015. Effect of standard heat treatment on the microstructure and mechanical properties of selective laser melting manufactured Inconel 718 superalloy. Mater. Sci. Eng. A 644, 32–40. doi:10.1016/j.msea.2015.06.021

Zhang, Y.N., Cao, X., Wanjara, P., Medraj, M., 2013. Oxide films in laser additive manufactured Inconel 718. Acta Mater. 61, 6562–6576. doi:10.1016/j.actamat.2013.07.039

Zhao, X., Chen, J., Lin, X., Huang, W., 2008. Study on microstructure and mechanical properties of laser rapid forming Inconel 718. Mater. Sci. Eng. A 478, 119–124. doi:10.1016/j.msea.2007.05.079

Zhong, C., Gasser, A., Kittel, J., Wissenbach, K., Poprawe, R., 2016. Improvement of material performance of Inconel 718 formed by high deposition-rate laser metal deposition. Mater. Des. 98, 128–134. doi:10.1016/j.matdes.2016.03.006

Zonglin, C., Shaogang, W., Weihong, L.I., 1997. Quantitative Phase Analysis of Inconel 718 by X-ray Diffraction. J. Mater. Sci. Lett. 16, 769–771. doi:10.1023/A:1018553703030

Figure captions

Fig. 1. Experimental setup of WAAM system (X-along wall length, Z-along wall height).

Fig. 2. Tensile coupon dimensions.

Fig. 3. (a) Final oxide layer formed on the topmost deposit in the normally built WAAM IN718 wall (b) oxide islands formed after one deposition on the oxide-free surface.

Fig. 4. SEM images of Zone A and B in Fig. 3 showing the oxide morphology. (a) Zone A (b) Zone B

Fig. 5. SEM images of the oxide layer at the top of the walls shown in Fig. 3 (yellow line in Fig. 3 indicates the sectioning position). (a) wall in Fig. 3a (b) wall in Fig. 3b

Fig. 6. Microhardness of the two comparative walls built with and without grinding.

Fig. 7. WAAM IN718 wall structure and the sample extraction positions.

Fig. 8. Mechanical testing results of the walls deposited with and without interpass grinding. (a) UTS and 0.2%YS (b) elongation

Fig. 9. Real thermal history during heat treatment. (a) solution (b) aging

Fig. 10. Inclusions observed in Wire B.

Fig. 11. TiN inclusion found in the fracture surface of the WAAM IN718 built using Wire B.

Fig. 12. Grain boundaries of IN718 produced by WAAM and wrought process. (a) WAAM (as deposited, half height of the wall) (b) wrought (solutionized)

Fig. 14. SEM images showing the precipitates morphology and distribution in the WAAM IN718 and wrought IN718 after aging. (a) WAAM (b) wrought